ARTICLES

Effects of traveling surface acoustic waves on neutron Bragg scattering from perfect crystals

W. A. Hamilton and M. Yethiraj
Solid State Division, Oak Ridge National Laboratory, Oak Ridge, Tennessee 37831
(Received 2 July 1998)

We have studied the effects of a traveling surface acoustic wave (SAW) disturbance on symmetric Bragg case neutron diffraction from a perfect crystal of lithium niobate. Generally, the reflectivity is increased as the SAW distortion creates an effective moving mosaic crystal in the near surface region. Unlike the corresponding x-ray situation in which the crystalline distortion is effectively stationary, thermal neutron and SAW velocities are comparable. Thus the interaction between the neutron and the coherent SAW phonons involves significant Doppler effects that also modify the reflected neutron intensity. While the observed effects can be explained qualitatively, as yet no quantitative picture exists of the interaction between the neutron and the coherent surface phonons in this situation. [S0163-1829(99)07105-2]

The effect of acoustic waves generated in single crystals on x-ray and neutron scattering has been studied for several decades now. For the most part these investigations have focused on bulk acoustic wave effects.[1–6] While more recently there have been studies on the effects of surface acoustic wave (SAW) distortions on Bragg diffracted x-ray intensities[7–9] the work presented in this report represents the first investigation of the corresponding neutron case. Further, since we used a device designed to produce a traveling SAW distortion with minimal standing-wave characteristics, it is a measurement of Bragg diffraction exploring the consequences of comparable velocities of the SAW and the diffracted radiation.

To a first approximation the expected effects on reflected neutron intensities are as follows: The distortion caused by the passage of a SAW of wavelength Λ and surface normal amplitude A, creates an effective crystal corrugational ''mosaic'' of spatial period Λ near the surface moving at the surface acoustic wave speed, v_S [Fig. 1(a)]. At the surface this corrugation will have an angular amplitude $\alpha = 2\pi A/\Lambda$, and an rms ''ripple mosaic'' width $\eta \sim \alpha/\sqrt{2}$. The SAW wavelength of our device is comparable to the primary extinction depth of the neutron reflection, while η is somewhat greater than the perfect crystal's total reflection Darwin width[10] (typically of order a few microradian). The distortion broadens the crystal's Bragg scattering interval and increases the reflected neutron intensity. We can consider the interaction as a Doppler-shift effect between the lab frame and the frame in which the SAW distortion mosaic is stationary. An earlier investigation of grazing incidence diffraction of cold neutrons reflected from the moving surface ''grating'' produced by a traveling SAW disturbance on quartz[11] showed significant Doppler effect magnifications of diffraction angles and diffracted intensities. In that case the nature of the material underlying the distorted reflecting interface was irrelevant since crystal lattice distortions have a neglible effect on the neutron optical Fermi pseudopotential of the quartz. In the more complicated large-angle situation considered here we found that Doppler effects can also dramatically modify the scattered Bragg intensity when thermal neutrons are reflected from the SAW distorted crystalline lattice region beneath a surface.

Surface waves were produced on a SAW delay line of conventional geometry by photolithographically etched interdigitated transducers[12] (IDT's) in aluminum configured upon a perfect single-crystal lithium niobate ($LiNbO_3$) substrate [Fig. 1(b)]. For a piezoelectric crystal such as $LiNbO_3$ the stresses induced on the surface when an oscillating voltage is applied to the IDT create a standing-wave deformation over the electrode region, resulting in a bidirectional SAW launch. $LiNbO_3$ is a trigonal crystal (hexagonally indexed).[13] The SAW surface normal for the device is the crystallographic b axis, while the SAW propagates along the c axis. In conventional SAW device terminology this is Y-cut $LiNbO_3$ with acoustic propagation in the Z direction.[14] This is a pure mode axis for this crystal, so the angle between phase and group velocities of the SAW is zero and therefore the acoustic power flow of our device is parallel to the acoustic wave vector and perpendicular to the SAW wave front. The SAW velocity for Y-Z $LiNbO_3$ is 3488 ms^{-1} and the periodicity of the IDT electrodes (hence the SAW wavelength) was 94 μm, at an operating frequency of 37 MHz. The SAW carrying area of the device was 5 mm, the width of the IDT, by 90 mm, the distance to the delay line's receiving transducer. To damp spurious SAW reflections the region behind the SAW generating transducer was mass loaded with a coating of neutron absorbing Gd_2O_3 paint. The receiving transducer was also painted over. Although this reduced its sensitivity, it eliminated acoustic Bragg reflections from its electrode pattern, which produced a back propagating SAW distortion, and consequently a standing-wave ''contamination'' of the traveling SAW distortion. Conventional ''laser probe'' measurements of grating diffraction of He-Ne laser light showed that the SAW amplitude varied linearly with the receiving transducer signal over the range of operation. This calibration was used to monitor the

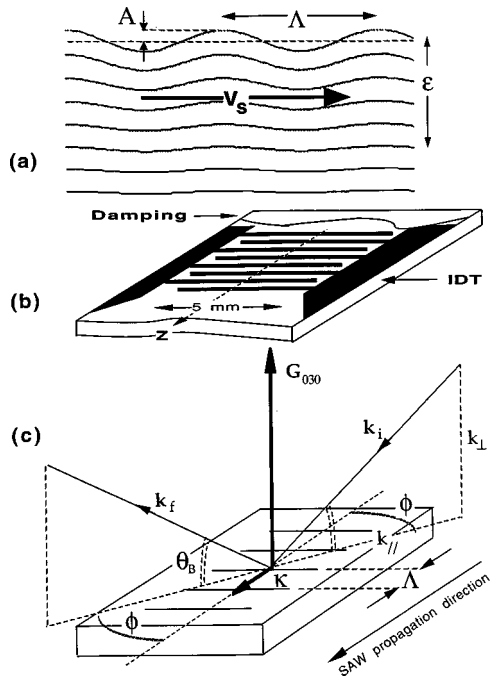

FIG. 1. (a) Surface acoustic wave distortion of a surface. (b) Schematic of SAW generating interdigital electrode pattern and Gd_2O_3 paint damping. (c) Schematic of SAW propagation on the $LiNbO_3$ surface with respect to the conventional scattering triangle. The scattering vector $\mathbf{G}_{030}$ is in the direction of the surface normal and is drawn at the point of incidence of the neutron beam to the surface, and hence along the ϕ rotation axis.

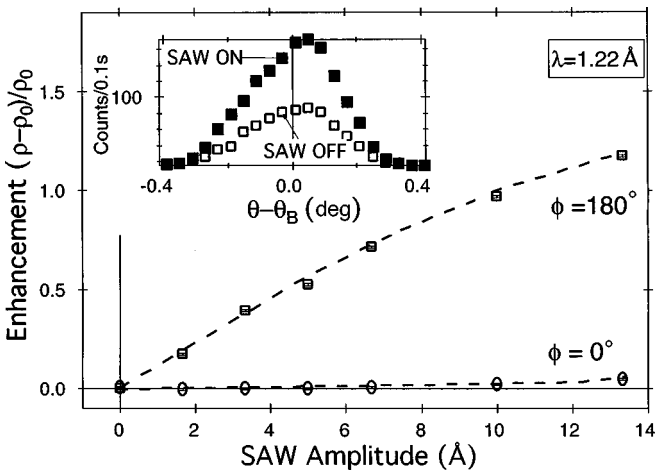

FIG. 2. Normalized enhancement of integrated reflectivity versus the SAW displacement amplitude at the surface for 1.22 Å neutrons for SAW propagation in the forward ($\phi=0°$, open circles) and backward directions ($\phi=180°$, open squares), with respect to the neutron beam. Inset shows the full rocking curve measurements for $\phi=180°$ at full SAW power (MURR data.)

SAW amplitude during our neutron measurements. At the maximum power (~200 mW) the device generated a displacement amplitude normal to the surface of 12–15 Å over the SAW carrying area.

Since the b axis is normal to the surface of our SAW device, $\{0k0\}$ reflections can be measured in the symmetric Bragg geometry, i.e., the reflection's reciprocal lattice vector, $\mathbf{G}$, is normal to the surface and to the SAW wave vector κ, of magnitude $\kappa=2\pi/\Lambda$. We denote the angle between the scattering plane and the SAW propagation direction as ϕ [Fig. 1(c)]. The neutron-diffraction measurements reported here used the 3XE triple axis at the Missouri University Research Reactor (MURR) and HB3 triple axis at the High Flux Isotope Reactor at Oak Ridge National Laboratory (ORNL) for a range of neutron wavelengths (0.81–2.44 Å) on the first allowed $\{0k0\}$ reflection for $LiNbO_3$, the (030) for which the lattice spacing d_{030} is 1.487 Å ($G_{030}=4.22$ $Å^{-1}$). The incident beam was produced by pyrolytic graphite monochromation with appropriate filters and had rms width $\delta\theta\sim0.15°$. The primary extinction depth for this Bragg reflection, Δ_{030}, is 38 μm. [$\Delta_{030}=\pi V_0/2d_{030}|F_{030}|$, where V_0 is the unit-cell volume and F_{030} is the (030) structure factor.] For a Y-Z $LiNbO_3$ SAW the penetration depth, ε, of the surface normal displacements is about 1.3Λ, ~120 μm in the present case, thus the SAW distortions extend several extinction depths into the crystal. At maximum power the rms angular width of the corrugational distortion of the surface is $\eta_{\max}\sim60\,\mu$rad. For the range of Bragg angles θ_B used in this work (~16°–35°), $\eta_{\max}$ is about an order of magnitude larger than the Darwin plateau width of the (030) reflection (in symmetric Bragg geometry), which is given by $\Delta\theta_0=2d_{030}\tan\theta_B/\Delta_{030}$, i.e. $\tan\theta_B\times7.8\,\mu$rad. From multiple reflection effects in dynamical crystal diffraction the integrated reflectivity of a perfect crystal in symmetric Bragg geometry saturates at a crystal slab thickness of about one extinction depth at the same value as would be achieved for the perfectly imperfect (mosaic) crystal described by kinematical theory for thickness of only Δ_G/π, i.e., in our case $\Delta_{030}/\pi\sim12\,\mu$m. The angular distortion of local crystal plane directions by greater than the Darwin width over several times these depths will greatly reduce these multiple reflection effects, creating an effective mosaic crystal rather thicker than Δ_{030}/π and with correspondingly higher integrated reflectivity.

The effective mosaic of a stationary corrugational distortion in the scattering plane $\eta|\cos\phi|$ is at a maximum when $\phi=0°$ or 180°. Although this is the case for x-ray diffraction from SAW, since the distortion is effectively stationary, the neutron case is very different. Figure 2 shows the dependence of measured normalized enhancement for (030) reflected 1.22 Å neutrons (Bragg angle $\theta_B=24.2°$) on SAW amplitude for SAW propagation towards $\phi=180°$ and away from the incident neutron beam direction $\phi=0°$. Clearly the Doppler effect on reflected neutron intensities is dramatic. For $\phi=180°$ SAW propagation, the enhancement at maximum SAW amplitude of ~13 Å more than doubles the observed integrated reflectivity. When the crystal is rotated to the $\phi=0°$ the orientation the enhancement is only 5%, a value reached in the $\phi=180°$ orientation for a SAW amplitude of only ~0.5 Å. A qualitative explanation of this effect is possible if we consider the analogous situation of neutron Bragg reflection from a mosaic crystal in motion parallel to the average lattice plane. Then, the phase space volume element selected by a reflection (angular sampling of the reflection) is increased by a Doppler factor equal to the ratio of the neutron velocity components parallel to the lattice planes in the reference frame in which the crystal is stationary and the lab frame.[15] In our case the frame in which the mosaic crystal is stationary corresponds to the frame in which the SAW

disturbance is stationary. The angular interval of a stationary ripple mosaic in the lab frame as projected onto the scattering plane, $\eta|\cos\phi|$, will be related to its value in the SAW stationary frame by a Doppler factor. Designating the SAW stationary frame by primes we find that the effective angular interval of the moving ripple mosaic is given by

$$\eta' = \eta|\cos\phi||(v_\parallel \cos\phi - v_S)/v_\parallel \cos\phi| \equiv \eta f_D(\phi),$$

where $v_\parallel$ is the neutron velocity component parallel to the surface and v_S is the SAW velocity and we have defined the Doppler magnification factor as

$$f_D(\phi) \equiv |(v_\parallel \cos\phi - v_S)/v_\parallel| = |\cos\phi - 2k_S/(G\cot\theta_B)|,$$

where k_S is the wave number of a neutron traveling at the SAW speed. Obviously this expression which properly relates only to the magnification of each infinitesimal volume sampled by the beam diverges as $v_\parallel \to 0$. If, however, we average over the phase-space width sampled by the beam, we obtain the following phase-space volume Doppler factor:

$$F_D \cong \{[(k_\parallel \cos\phi - k_S)^2 + (\delta k_\parallel \cos\phi)^2]/(k_\parallel^2 + (\delta k_\parallel)^2]\}^{1/2},$$

where $k_\parallel$ is the neutron wave vector component parallel to the surface. Note that for a given reflection the phase-space width sampled by the neutron beam is constant between frames for constant beam collimation $\delta\theta$, since $\delta k_\parallel \approx \delta\theta\, G/2 = 6\times10^{-3}\,\text{Å}^{-1}$. For the cases considered here instrumental limitations keep us relatively far from normal incidence so $\delta k_\parallel$ is small relative to $k_\parallel$ and to the accuracy of our measurements $F_D \cong f_D$ and we will use the simpler f_D expression in most of the discussion to follow. These Doppler factors are greatest when the SAW velocity is in the opposite sense to the neutron velocity, so we may expect maximum apparent mosaic and hence enhancement of reflected neutron intensity when $\phi = 180°$. For $v_\parallel < v_S$ the enhancement will be a minimum for when the velocities are in the same direction, when $\phi = 0°$. However, for $v_\parallel > v_S$, a zero enhancement minimum would be expected for $\phi \approx \pm\arccos(v_S/v_\parallel)$ since $f_D = 0$. In this case we now expect a local maximum at $\phi = 0°$. The SAW distortion's effect in Doppler enhanced wave-vector acceptance normal to the surface will be

$$\Delta k_\perp' \approx \eta' k_\parallel = f_D \eta k_\parallel = \eta(\pi/d_{030}) f_D \cot\theta_B.$$

For $\phi = 0°$ and $\phi = 180°$ we note that $f_D \cot\theta_B$ is simply the cotangent of the Bragg angle in the frame where the SAW distortion is stationary. The Darwin plateau (100%) halfwidth of the undistorted perfect-crystal reflectivity expressed as a wave number is simply $\Delta k_\perp^0 = 2\pi/\Delta_{030}$ in any frame. Beyond this range the reflectivity falls rapidly and the full integrated reflectivity of a perfect crystal Bragg reflection ρ_0 is equivalent to unit reflectivity over a range of only 1.33 $\Delta k_\perp^0$. When the SAW distorted crystal acceptance $\Delta k_\perp'$ exceeds $\Delta k_\perp^0$ neutrons will be reflected from the surface region that would not have been reflected by the undistorted perfect crystal giving an enhanced integrated reflectivity. When by reason of decreased SAW distortion amplitude or Doppler reduction ($f_D \ll 1$) $\Delta k_\perp'$ is less than $\Delta k_\perp^0$ the observed reflectivity in our experiments will be essentially the same as for the undistorted crystal.

An equivalent expectation is reached if we consider the change in the incident perpendicular neutron wave vector associated with the creation/absorption of n surface (SAW) phonons of wave vector $\kappa \equiv 2\pi/\Lambda$, which is easily shown to be

$$\Delta k_\perp(\pm n) = \pm n\kappa(k_\parallel \cos\phi - k_S) + n^2\kappa^2/2G \sim \pm n(\kappa/2) f_D \cot\theta_B, \quad \text{since} \quad \kappa \ll G.$$

The number of surface phonon creation or absorption events required to scatter a neutron which would not be reflected otherwise, n^0, is therefore given by

$$n^0 \sim 2(\Lambda/\Delta_G)/(f_D \cot\theta_B) \approx 5/(f_D \cot\theta_B).$$

As in the Doppler treatment, the enhancement will be increased as $f_D \cot\theta_B$ increases and the number of phonons events necessary to scatter a neutron that is not within the perfect crystal acceptance decreases.

For the 1.22 Å ($\theta_B = 24.2°$) data shown in Fig. 2, $v_\parallel = 2960\,\text{ms}^{-1}$ so $v_\parallel/v_S = 0.85$ and f_D changes by about an order of magnitude between the $\phi = 180°$ and $\phi = 0°$, from 2.2 down to 0.2. For the SAW wavelength of our device and the extinction depth of the (030) reflection $2(\Lambda/\Delta_{030}) \sim 5$. At maximum SAW amplitude $\eta = \eta_{\max}$, the ratio of the SAW distorted and perfect-crystal acceptances at the surface $\Delta k_\perp'/\Delta k_\perp^0 = (f_D \eta \Delta_{030}/2d_{030})\cot\theta_B$ varies from ~ 40 at $\phi = 180°$ down to ~ 4 at $\phi = 0°$ (while n^0 changes from ~ 1 to ~ 12). Clearly for $\phi = 180°$ the SAW distortion has created an effective mosaic crystal at the surface. For $\phi = 0°$ the neutron beam comes close to pacing the distortion so f_D is small and the Doppler effect has greatly reduced the effective amplitude of the distortion and the enhancement is consequently very much weaker.[16]

An adequate theoretical treatment of the dependence of the integrated reflected intensity on the SAW distortion parameters would require a detailed treatment of both dynamical diffraction and the neutron transport effects over the distorted crystal region, and as such is well beyond the scope of this paper. Since the distortion extends only a few primary (dynamical) extinction depths into the crystal and is coherent the normal mosaic crystal transport theory model which assumes randomly oriented mosaic blocks rather smaller than an extinction depth in size cannot be applied. Adaptation of dynamical diffraction theory to coherent distortions varying over the length scale of the extinction depth is also intractable. To first order we might reasonably expect the normalized enhancement of the scattered intensity to go as a monotonically increasing function of the ratio $(\Delta k_\perp'/\Delta k_\perp^0)$, i.e., at constant SAW power as $f_D(\phi)\cot\theta_B$.

The choice of a reciprocal lattice vector **G** perpendicular to the surface allows mapping out the Doppler dependence of the reflected intensity with ϕ without altering the scattering geometry by rotating the crystal about the scattering vector.[17] A series of measurements of the full ϕ dependence of enhancement observed at our maximum SAW power ($\langle A\rangle \sim 13$ Å) at a range of Bragg angles is shown in Fig. 3. The data were taken at neutron wavelengths of 0.81 and 1.53 Å, where at the Bragg condition $v_\parallel$ is respectively about 35% greater or less than v_S, and at 1.06 Å, where $v_\parallel$ exactly matches the SAW velocity. The incident neutron beam was

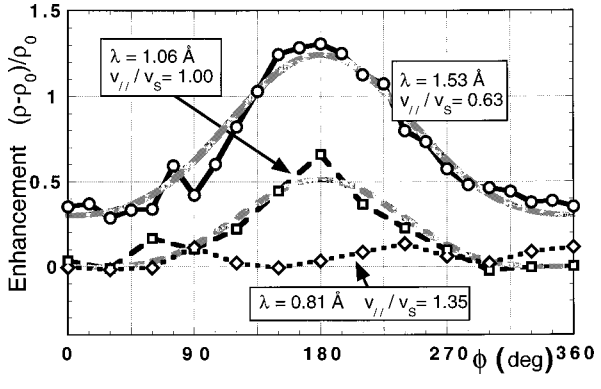

FIG. 3. Normalized enhancement of integrated reflectivity at full SAW power ($\langle A\rangle \approx 13$ Å) versus the SAW propagation angle ϕ for wavelengths chosen such that the magnitude of the incident neutron velocity component parallel to the surface is greater than ($v_\parallel/v_S = 1.35$, open diamonds), less than ($v_\parallel/v_S = 0.63$, open circles) and equal ($v_\parallel/v_S = 1$, open squares) to the SAW speed. The gray lines in Fig. 3 show a variation of $f_D^2(\phi)$ for these last two cases, $|\cos\phi - 1/0.63|^2$ and $|\cos\phi - 1|^2$, respectively, in both cases rescaled in amplitude and mean to the magnitude of the observed enhancements (HFIR-ORNL data.)

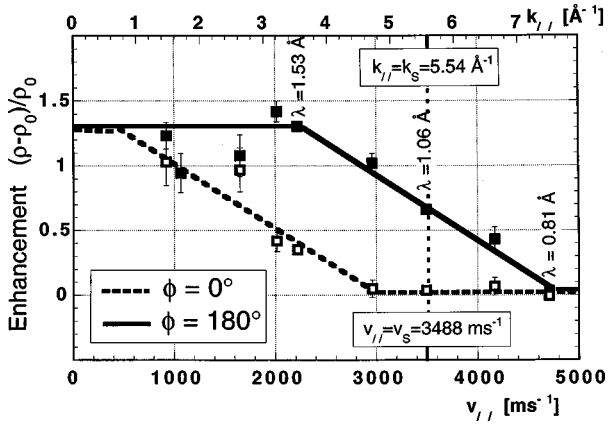

FIG. 4. Normalized enhancement of integrated reflectivity at full SAW power ($\langle A\rangle \sim 13$ Å) at a range of wavelengths versus magnitude of the incident neutron velocity component parallel to the surface, for SAW propagation in the forward ($\phi = 0°$, open squares) and backward directions ($\phi = 180°$, solid squares). Lines are a guide to the eye only (HFIR-ORNL data.)

collimated to a cross section of 1.5×1.5 mm at the sample surface, so that its footprint was within the ~ 5 mm width of the SAW carrying region for the full range of ϕ.

Qualitatively the 1.06 and 1.53 Å, data show the ϕ dependence of the enhancement varying with $f_D(\phi)$, approximately as one would expect. The gray lines in Fig. 3 show a variation of $f_D^2(\phi)$ for these wavelengths, in both cases rescaled in amplitude and mean to the magnitude of the observed enhancements, which was found to follow the data fairly closely. For 1.06 Å ($\theta_B = 20.9°$) and $\phi = 0°$ where the Doppler factor f_D zero (the volume averaged value $F_D \sim \delta k_\parallel / k_\parallel \ll 1$) and the observed enhancement is zero to within experimental error. The effect on the observed intensity being interpretable either as the Doppler effect diminishing the effective SAW mosaic or, in the surface phonon treatment, as the divergence of n^0 as $f_D \cot\theta_B \to 0$. At $\phi = 180°$ f_D is at a maximum of 2 and there is a corresponding maximum enhancement of $\sim 70\%$ ($n^0 \sim 0.95$). When $v_\parallel$ is rather less than v_S, the minimum Doppler factor is greater than unity and the relative overall variation of the enhancement with ϕ is smaller. For 1.53 Å ($\theta_B = 31.0°$) the scattering is significantly enhanced for all ϕ. The ratio of the enhancements in the forward $\phi = 0°$ and backward ($\phi = 180°$) direction is $\sim 0.35/1.3 = 0.27$, close to the ratio of the corresponding Doppler factors $0.59/2.59 = 0.23$, as we would expect from the moving ripple mosaic analogy, while the corresponding variation in n^0 is from ~ 5 down to ~ 1.1. However, we note that while the ratios of Doppler and n^0 values are approximately consistent with the variation of enhanced reflected intensity with ϕ at these two wavelengths considered individually, this is not true for the relationship between wavelengths. Instead of generally increasing with decreasing wavelength, as $\cot\theta_B$ becomes larger at smaller Bragg angles the observed enhancement has decreased. This is obvious from consideration of the data for 0.81 Å ($\theta_B = 15.8°$), for which the enhancement is surprisingly small for all ϕ, less than about 10%, which is comparable to the systematic errors ($\pm 4\%$) in the measurement at this wavelength.[18] For $\phi = 180°$, the value of n^0 for 0.81 Å neutrons is ~ 0.8, somewhat less than the corresponding values for 1.06 and 1.53 Å. However, while fewer SAW phonons would now need to be created or absorbed to scatter a neutron out of the Darwin width than at either of the longer wavelengths it is clear that the enhancement and hence the strength of the neutron surface phonon interaction falls fairly rapidly with decreasing Bragg angle counteracting the increase in $\Delta k'_\perp / \Delta k^0_\perp$.

The overall dependence of the enhancement observed at full SAW power with $v_\parallel$ (equivalently $k_\parallel$), for the $\phi = 0°$ and $\phi = 180°$ orientations over a series of wavelengths ranging from 2.44 Å down to 0.81 Å, is shown in Fig. 4. Qualitatively the ϕ dependence is, to some extent, what we would expect: At longer wavelengths, since $v_\parallel$ is rather less than v_S, the variation in the enhancement becomes less dependent on the direction of SAW propagation and plateaus (more than doubling the integrated scattered intensity) becoming independent of the SAW propagation direction (ϕ) at the backscattering condition $\lambda = 2d_{030}$ for which $v_\parallel = 0$, and $f_D = v_S/v_\parallel$. The maximum enhancement *ratio* between backward and forward senses of the neutron velocity does occur near the pacing condition $v_\parallel = v_S$. However, at shorter wavelengths although the Darwin width continues to decrease the enhancement due to the SAW mosaic rapidly decreases and has become negligible for 0.81 Å neutrons.

This falloff in observed enhancement is most probably due to bending of our 100-mm-long×2-mm-thick SAW device. As demonstrated by White[19] for x rays, a statically bent crystal can exhibit a range of scattering behavior from perfect-crystal dynamical diffraction to perfectly imperfect (mosaic) kinematic diffraction. Primary extinction is eliminated and the kinematical reflectivity limit is achieved for a bent crystal when in penetrating a crystal to about one extinction depth the curvature changes the angle of incident radiation to the crystal planes more than one Darwin width from their value at the surface (the Bragg angle). Using the White's geometrical arguments for the symmetric Bragg

case, we may therefore expect the perfect nature of a crystal to be disrupted by curvature of radius R, such that:

$$R\Delta\theta_0/(\Delta_G/\pi)\sim\cot\theta_B \Rightarrow R\sim(\Delta_G^2/2d_G)\cot^2\theta_B .$$

In the present case, R is 60 m for 0.81 Å neutrons and 10 m for 2.44 Å. A radius of curvature of order 60 m, while bending our device by only 0.1° over its 100 mm length, could render the the relectivity of for 0.81 Å neutrons essentially kinematical, while 2.44 Å neutron reflection would be largely dynamical. In the former case the enhancement effect will disappear since the crystal cannot be made more than perfectly imperfect by the SAW distortion.

In conclusion, we have shown that treating a SAW distortion as a moving mosaic crystal accounts reasonably well for the observed rotational Doppler effects in this study of the influence of SAW's on the enhancement of Bragg diffracted neutron intensity. The falloff in the observed enhancement at shorter wavelengths seems consistent with the effects of crystal curvature due to static strains of the device mounting or possibly heating effects when it is operated. A particular consequence of this falloff, however, is that we were unable to verify the expectation that for $v_\parallel > v_S$ enhancement minima should appear at $\phi \approx \pm \arccos(v_S/v_\parallel)$, with a local maximum appearing at $\phi = 0°$.

Thanks are due to A. G. Klein, G. I. Opat, and A. Cimmino, University of Melbourne, S. A. Werner, University of Missouri-Columbia, and H. Sabine and D. Reynolds, Australian Telecom Research Laboratories. X-ray measurements confirming some results of previous investigators were made with the help of J. Budai of the ORNL Solid State Division. This research was supported in part by the USDOE under Contract No. DE-AC05-96OR22464 with Lockheed Martin Energy Research Corporation.

[1] W. J. Spencer, Appl. Phys. Lett. **2**, 133 (1963).

[2] T. F. Parkinson and M. W. Moyer, Nature (London) **211**, 400 (1966).

[3] A. G. Klein, P. Prager, H. Wagenfeld, P. J. Ellis, and T. M. Sabine, Appl. Phys. Lett. **10**, 293 (1967).

[4] R. Michalec, L. Sedlakova, B. Chalupa, D. Galociova, and V. Petrzilka, Acta Crystallogr., Sect. A: Cryst. Phys., Diffr., Theor. Gen. Crystallogr. **27**, 410 (1971), and references therein.

[5] R. Köhler, W. Möhling, and H. Peibst, Phys. Status Solidi **41**, 75 (1970); Phys. Status Solidi B **61**, 173 (1974); **61**, 439 (1974).

[6] L. D. Chapman, R. Colella, and R. Bray, Phys. Rev. B **27**, 2264 (1983).

[7] S. Kikuta, T. Takahashi, and S. Nakatani, Jpn. J. Appl. Phys., Part 2 **23**, L193 (1984).

[8] B. Sander, E. Zolotoyabo, and Y. Komen, J. Phys. D **28**, A287 (1995).

[9] E. Zolotoyabo and I. Polykarpov, J. Appl. Crystallogr. **31**, 60 (1998).

[10] The neutron optical concepts used in this paper are fully discussed in V. F. Sears, *Neutron Optics* (Oxford University, New York, 1989). Kinematical (imperfect or mosaic crystal) and dynamical (perfect crystal) neutron Bragg diffraction are specifically discussed in Chaps. 5 and 6.

[11] W. A. Hamilton, A. G. Klein, G. I. Opat, and P. A. Timmins, Phys. Rev. Lett. **58**, 2770 (1986). The closest analogy for this experiment is an optical reflection grating. To our knowledge the corresponding experiment has not been performed for x rays.

[12] R. M. White and F. W. Voltmer, Appl. Phys. Lett. **7**, 314 (1965); discussions of most aspects of piezoelectric crystal SAW generation and device technology are covered in *Acoustic Surface Waves*, edited by A. A. Oliner, Springer Topics in Applied Physics Vol. 24 (Springer, Berlin, 1978).

[13] R. W. G. Wyckoff, *Crystal Structures*, 2nd ed. (Wiley, New York, 1964), Vol. 2, Chap. VIIA, p. 422.

[14] B. A. Auld, *Acoustic Fields and Waves in Solids* (Wiley, New York, 1973), Vol. II, Appendix 4C.

[15] G. S. Bauer and R. Scherm, Physica B & C **136**, 80 (1986).

[16] The neutron intensity actually falls by ~0.5% at $\langle A\rangle = 2.5$ Å. Similar effects have been seen for low power SAW distortions in x-ray studies (see Ref. 8) and were interpreted as due to release of intrinsic surface strains.

[17] The incident beam was restricted to the SAW carrying surface either by Cd masking the crystal surface region on either side of the 5 mm SAW width (MURR) or by pinhole collimation of the beam to restrict the incident footprint at the Bragg angle on the crystal surface to within this width (ORNL). Both methods were equivalent.

[18] The SAW on and off rocking curve measurements were therefore performed several hours apart and the observed intensity was apparently sensitive to instrumental drifts over this time scale for lower Bragg angles. A repeat of the rocking curve measurements at $\phi = 0°$ immediately after this run gave an enhancement of 0.3%, rather than the 10% enhancement plotted at $\phi = 360°$.

[19] J. E. White, J. Appl. Phys. **21**, 855 (1950).